EGU General Assembly
2025, Vienna, Austria **(EGU25-1828)**

Hydraulic conductivity estimation in Porous Media: Insights from Neural computing

Abhishish Chandel[1], Vijay Shankar[2]
[1]*Faculty member, National Institute of Technology, Hamirpur, India*
[2]*Associate Professor, National Institute of Technology, Hamirpur, India*
Email: abhishishchandel@gmail.com, vsdogra12@gmail.com

Abstract

Precise estimation of hydraulic conductivity (K) in porous media is vital for advancing hydrological and subsurface flow investigations. Groundwater experts have increasingly adopted neural computing approaches to indirectly determine K in porous media, offering a more efficient alternative to conventional methods. The research focuses on developing the Feed-Forward neural network (FFNN) and Kohonen Self-organizing maps (KSOM) models to compute the K using easily measurable porous media parameters i.e., grain-size, uniformity coefficient, and porosity. The observed data were split into 70% and 30% for the development and validation phase, respectively. The developed model's performance was examined via statistical indicators, including root mean square error (RMSE), determination coefficient (R^2), and mean bias error (MBE). The findings suggest that the FFNN model significantly outperforms the KSOM model in estimating the K value, with the KSOM model achieving only moderate accuracy. During the validation phase, the FFNN model shows a stronger correlation with the measured values, yielding RMSE, R^2, and MBE values of 0.016, 0.94, and 0.006, while the KSOM model returns values of 0.024, 0.91, and -0.004 respectively. The FFNN model's superior predictive ability makes it a reliable tool for accurate K estimation in aquifers.

Keywords: Hydraulic conductivity, KSOM, FFNN, Porosity.

Introduction

For porous media, an accurate assessment of hydraulic conductivity (K) is fundamental for the analysis of aquifers and subsurface flow processes (Lee *et al.* 2015). Hydraulic conductivity measures the ease of fluid particle movement through the voids of the soil mass (Lu *et al.* 2012). The key independent variables that govern the K of porous media include particle uniformity, porosity, compaction density, and grain-size (Wang *et al.* 2017). For the measurement of K, numerous direct and indirect techniques can be utilized. Direct techniques encompass a range of experimental and field methods, including the Permeameter tests (Constant and Falling head), and the Guelph permeameter & pumping test (Pucko & Verbovsek 2015). The difficulty in assessing K in the field arises from inadequate insight into the hydraulic boundaries and aquifer characteristics (Chandel *et al.* 2022b). In contrast, experimental K approaches are hindered by the difficulty of collecting samples that accurately represent the in-situ field condition of soil mass (Riha *et al.* 2018).

As a result, indirect techniques i.e., empirical equations & data-driven approaches, emerged and gained prominence for estimating the K of porous media using readily measurable properties (Akbulut 2005). The use of empirical equations is limited to their intended domains, as they were formulated under specific conditions, which may lead to random inaccuracies in K calculations (Odong 2007; Chandel & Shankar 2022).

In recent decades, the use of data-driven approaches has expanded across numerous areas of hydraulic and groundwater engineering (Williams & Ojuri 2021). These approaches excel in carrying out the complicated tasks of modeling, training, and validating data points, which are attained from laboratory work (Thakur *et al.* 2022). These approaches are categorized into supervised learning, which relies on defined input and output data pairs, and unsupervised learning, where input and output data pairs are not specified (Sen *et al.* 2019). The enhanced prediction efficacy of these techniques, compared to traditional methods, has led to their widespread adoption across various domains of irrigation, hydraulics, and groundwater engineering (Kumar et al. 2020).

Neural computing models incorporating Artificial Neural Networks (ANN) and Adaptive Neuro-Fuzzy Inference Systems (ANFIS) were developed by Yilmaz et al. (2012) using distinct grain diameters (d_{10}, d_{30}, & d_{60}) to estimate the K of granular media. The study's findings suggest that the ANFIS model exceeds the performance of the ANN model in calculating the K value. The effectiveness of three predictive models i.e., ANFIS, ANN, and Multiple linear regression (MLR) has been explored by Arshad et al. (2013) in calculating the K value. The evaluation of statistical measures highlights the superior performance of the ANFIS model compared to the other two models. The efficacy of ANFIS, ANN, and Support Vector Machine (SVM) was investigated by Naganna and Deka (2019) who suggested that the ANFIS and ANN technique estimates the K closer to the measured values. Williams & Ojuri (2021) compared two techniques i.e., MLR and Feed Forward Neural Network (FFNN) to compute the K value of coarse soil media. Using six input variables for model development, the study reveals through statistical analysis that the FFNN model provides a better prediction of K compared to the MLR model.

Although supervised algorithms offer powerful prediction capabilities, missing outliers in the data can undermine their predictive performance (Kumar *et al.* 2020). In contrast, the KSOM based on unsupervised learning, clusters high-dimensional data into a smaller grid map, revealing the inherent relationships among the involved parameters (Kohonen *et al.* 1996). The clustering process enables the effective replacement of missing values using the map's characteristics, preventing any disruption in model predictions (Kumar *et al.* 2020). Existing literature indicates that the KSOM has not yet been applied to compute the K of granular media. Besides KSOM, a few researchers have used the FFNN to determine the hydraulic conductivity value based on various grain-size parameters. In terms of their influence on K, the uniformity coefficient, porosity, and grain-size are regarded as independent variables in model development. The main aims of the study are:

1. To develop and validate models using FFNN and KSOM techniques to determine the K of porous media from measurable grain-size parameters.
2. To examine the efficacy of the FFNN, and KSOM models in estimating K using various statistical indicators.

Materials and Methodology

Porous media used and Experimental procedure

This study involved collecting 165 soil samples from the banks of the Beas River in Kangra District, Himachal Pradesh, India (31°43′N, 75°32′E), for experimental work. Soil samples were extracted using a thin-walled sampler, designed with a 100 cm penetration length and an 8.5 cm cross-sectional diameter. The composition of the collected soil samples included coarse & fine sands, gravel, and silt proportions. Grain-size analysis, performed according to ASTM (2007) guidelines, was the initial step to assess the grain-size characteristics, yielding values for d_{10}, d_{30}, d_{50}, and d_{60} (indicating grain-size at 10%, 30%, 50%, and 60% finer by weight). The specific gravity of the soil samples, vital for porosity calculation, was computed through the pycnometer method. Furthermore, K tests were conducted on the soil samples using a constant head permeameter (Figure 1) with diameters of 5.08, 10.16, and 15.24 cm.

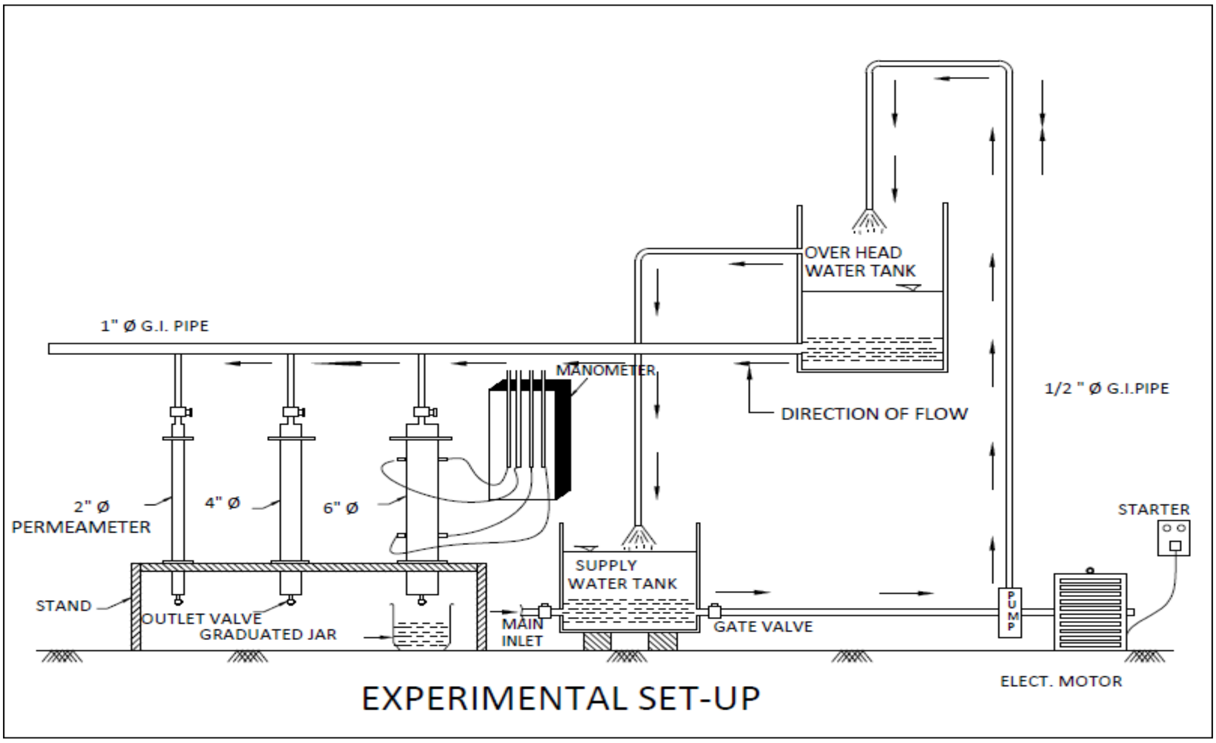

Figure 1. Set-up for measuring the K of soil samples.

A line diagram indicating the K measurement arrangement is presented in Figure 1, featuring components such as manometers, water supply & overhead water tank, and permeameters. The permeameters, made from galvanized iron pipes, feature a total and test length of 1 m and 0.46 m, respectively. The permeameter includes pressure-tapping ports positioned around its periphery at regular intervals of 0.46 m to measure head differences. A constant head is maintained by an overhead water tank elevated 2.50 m above the ground, which is continuously replenished by water from the recirculating tank below. The collected soil sample's K was determined using the standard procedure referenced in ASTM (2006). Water temperature was monitored via a digital thermometer during the experiments, and the K of the porous media samples was calculated using Darcy's equation (Qiu & Wang, 2015). The observations collected through experiments were used to develop the FFNN and KSOM models. For model development, different independent parameters i.e., porosity (n), uniformity coefficient (U), and grain-size (d_{10} & d_{50}) were employed in this study. The use of three distinct permeameter diameters in the experimental work provided a total of 495 observations from 165 soil samples. The next section covers the data-driven techniques applied in the study for modeling purposes.

Feed-Forward Neural Network (FFNN)

The FFNN, which is the most popular artificial neural network, undergoes successive forward and backward passes to achieve minimal error (Dawson & Wilby 2001). The FFNN architecture, depicted in Figure 2, comprises three layers: input, hidden, and output. The training process allows the model to store information related to the network architecture and its synaptic weights. Based on the model's training experience, the model predicts the output when provided with new input data. The parameters were scaled between -1 and +1 before being introduced to the network as input data.

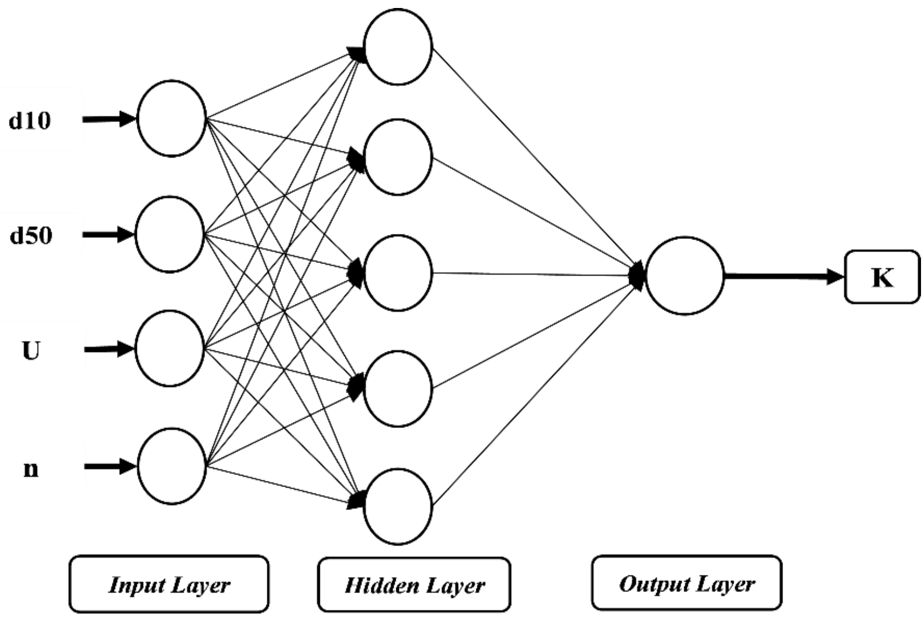

Figure 2. Architecture of the FFNN model utilized in the study.

In the FFNN model, the hidden layer neurons were configured with the sigmoid activation function, and the output layer neurons were set to use a linear activation function. The selection of the best-performing network involves a trial-and-error strategy, specifically by testing the FFNN model with 10 hidden neuron configurations. The trial-and-error strategy is adopted to optimize the correlation between training datasets and minimize errors, using the smallest possible number of hidden neurons to mitigate overfitting risks. Figure 2 depicts the most effective FFNN architecture identified in the present work, containing 5 hidden neurons. The training network was optimized using the Levenberg-Marquardt learning algorithm, chosen for its high convergence efficiency and reduced residuals (Kumar *et al.* 2020). The development and validation of the FFNN model were carried out in Matlab R2024a, adhering to the methodology illustrated in Figure 3.

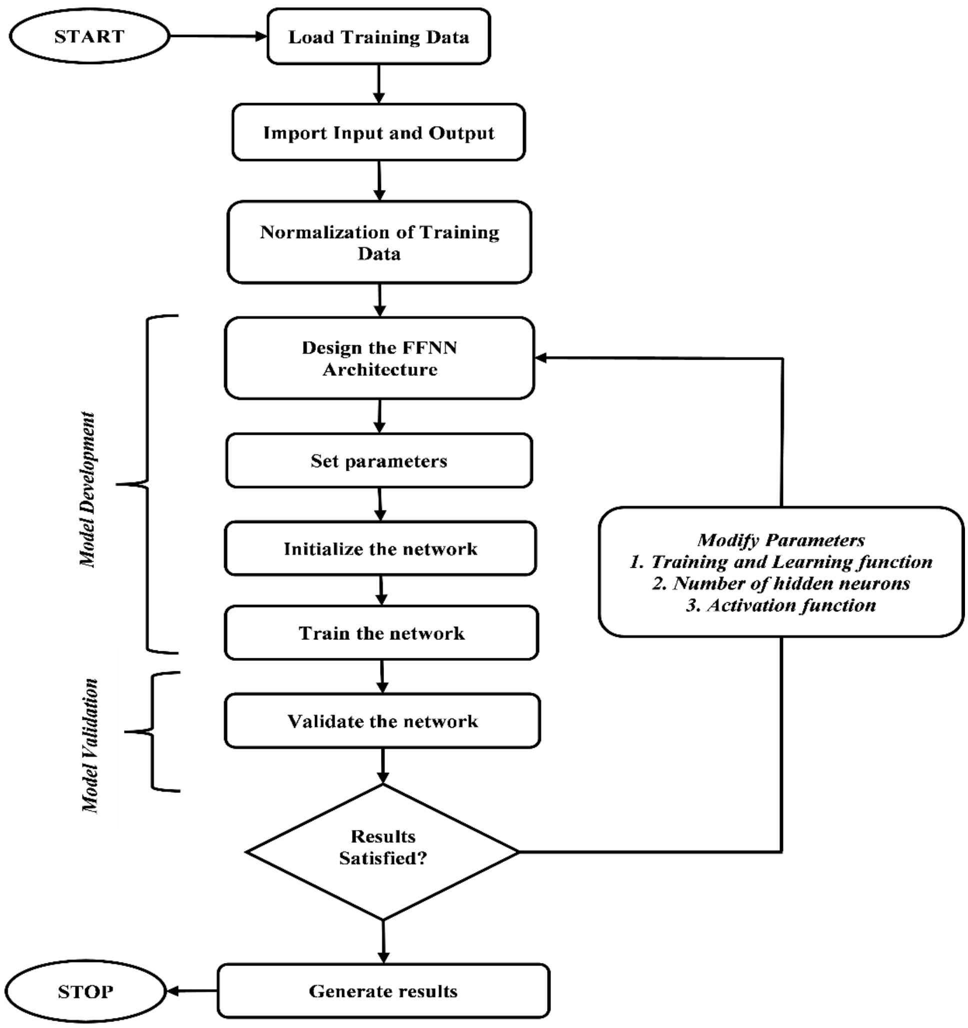

Figure 3. Flowchart depicting the approach employed for FFNN modelling.

Kohonen Self-Organizing Maps (KSOM)

The KSOM is a prominent unsupervised neural network model. Through clustering, it converts complex multidimensional data into a concise relationship. The input signal is optimized through unsupervised competitive learning using the neurons present on the Kohonen map (Kohonen *et al.* 1996). The input data is clustered to produce a pattern that resembles the output or its adjacent unit (Rustum & Adeloye 2007). As depicted in Figure 4, the KSOM consists of an interconnected high-dimensional input layer and a low-dimensional output layer. In the output layer, a grid of M neurons is arranged in two dimensions and the set of data points in these neurons is identical to those in the input vector.

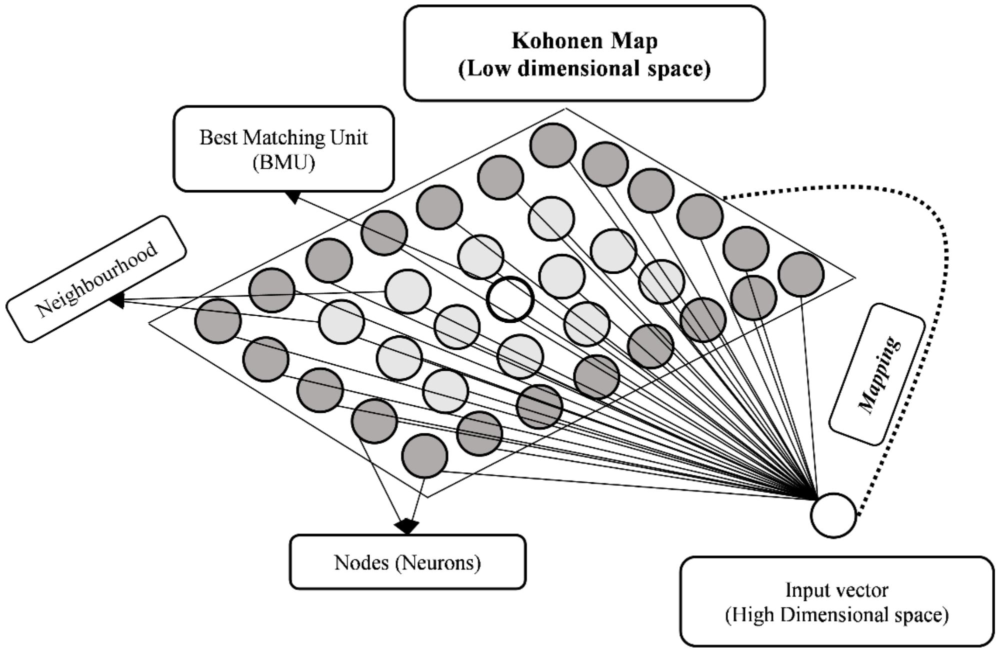

Figure 4. Diagram illustrating the BMU in a KSOM.

The equation (1) is used to determine the M value i.e., neurons in the output layer (Garcia & Gonzalez 2004).

$$M = 5 \times X^{1/2} \quad (1)$$

where, X indicates the entire dataset in the training phase.

The KSOM training begins by normalizing the input dataset, equalizing the influence of each variable on the map's structure. Subsequently, a randomly selected normalized input vector is picked and presented to each neuron displayed on the map. The KSOM uses Euclidean Distance (ED) as a measure to locate the code vector closest to the input vector (Rustum & Adeloye 2007). Figure 4 illustrates that the neuron corresponding to the lowest ED value is termed the winning neuron or Best Matching Unit (BMU). While the KSOM is capable of model identification, generalization of the dataset, and prediction purposes (Kumar et al., 2021), this study focuses on its application for K prediction, as illustrated in Figure 5.

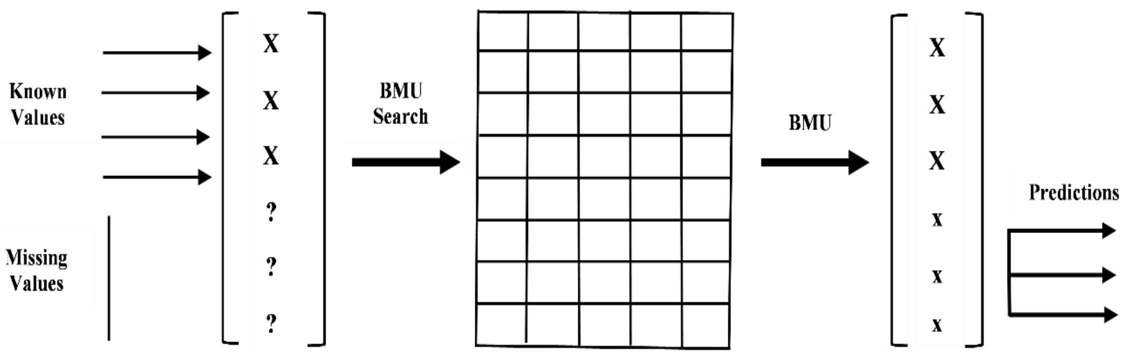

Figure 5. KSOM-based prediction of the missing values within the input vector.

The KSOM model is initially formulated by utilizing the input vectors from the training data. The K values, which were either removed or missing from the validation dataset (presented in Figure 5), are subsequently provided to the KSOM to find the BMU. The corresponding values in the BMU were utilized to compute the missing K values. The development and validation of the KSOM model were carried out in Matlab R2024a, adhering to the methodology illustrated in Figure 6.

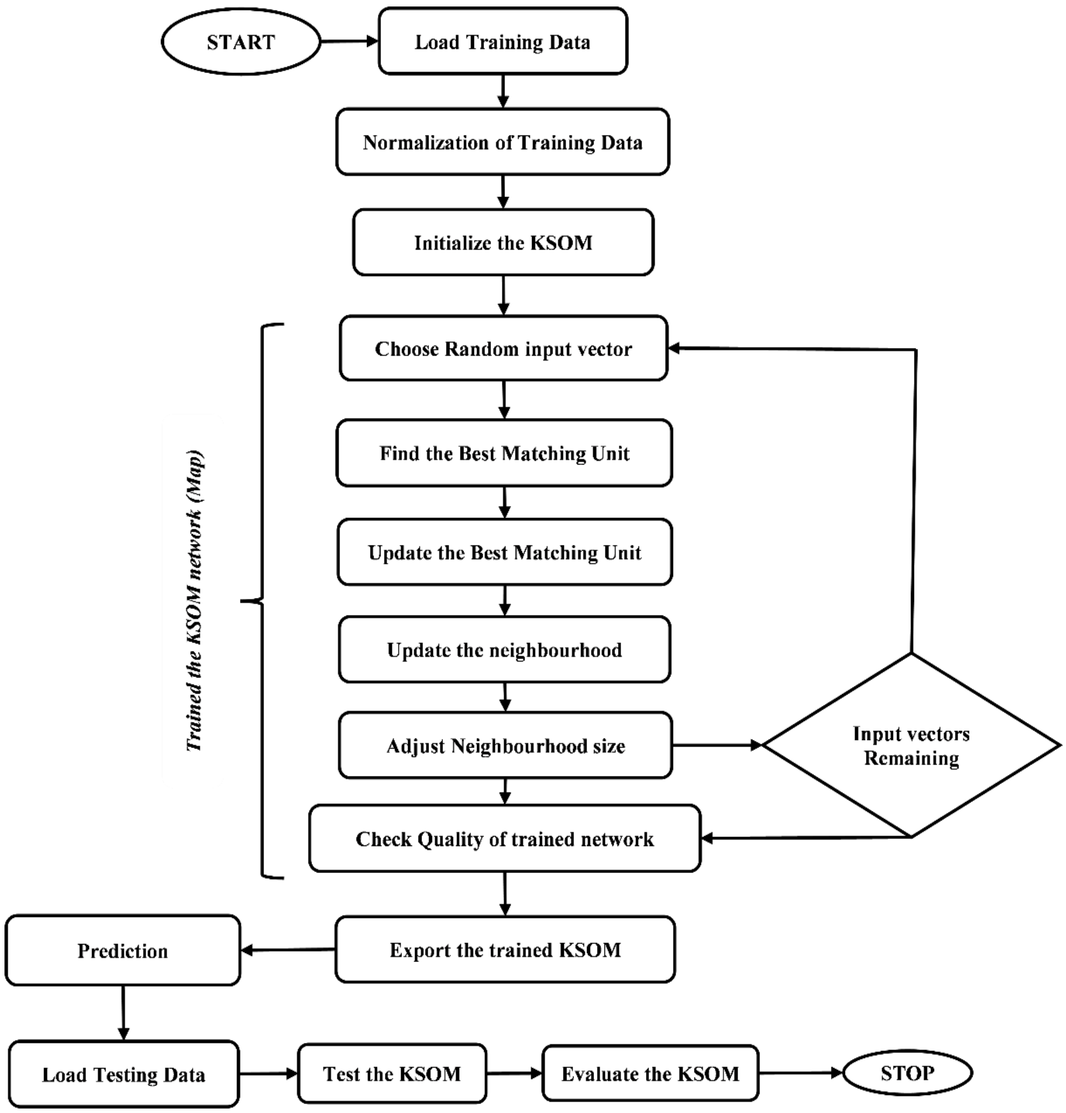

Figure 6. Flowchart depicting the approach employed for KSOM modelling.

Model evaluation using statistical analysis

The prediction capability of the FFNN and KSOM models for K computation was evaluated through statistical indicators, including determination coefficient (R^2), root mean square error (RMSE), agreement index (AI) mean bias error (MBE), scatter index (SI), and mean absolute error (MAE) (Chandel *et al.* 2022a). Also, the regression line's significance was tested using the analysis of variance (ANOVA) method. The different statistical indicator equations are:

$$R^2 = \left[\frac{\sum_{i=1}^{m}(a_i - \bar{a})(f_i - \bar{f})}{\sqrt{\sum_{i=1}^{m}(a_i - \bar{a})^2 \sum_{i=1}^{m}(f_i - \bar{f})^2}} \right]^2 \quad (2)$$

$$RMSE = \sqrt{\frac{\sum_{i=1}^{m}(a_i - f_i)^2}{m}} \quad (3)$$

$$AI = 1 - \frac{\sum_{i=1}^{m}(f_i - a_i)^2}{\sum_{i=1}^{Z}|f_i - \bar{a}| + |a_i - \bar{a}|} \quad (4)$$

$$MBE = \sum_{i=1}^{m} \frac{1}{m}(f_i - a_i) \quad (5)$$

$$SI = \frac{\sqrt{\frac{1}{m}\sum_{i=1}^{m}(f_i - a_i)^2}}{\bar{a}_i} \quad (6)$$

$$MAE = \frac{1}{m}\sum_{i=1}^{m}|a_i - f_i| \quad (7)$$

where, a_i & f_i represent the measured and predicted K values respectively, $\bar{a}$ & $\bar{f}$ indicates the average value of measured and predicted K respectively, and m is the entire dataset. The model exhibits a stronger agreement with the measured data when AI and R^2 are closer to 1, and MAE, SI, RMSE, and MBE are minimized (Naeej *et al.* 2017).

Results and Discussion

This study uses the grain-size characteristics, which are straightforward to measure, alongside the experimental data to develop the FFNN and KSOM models. The study begins with an overview of the statistical analysis and dataset employed for developing and validating the models, followed by a section that focuses on K determination using the developed models and quantitatively evaluating their performance with statistical indicators.

Statistical analysis

The different grain-size characteristics namely d_{10}, d_{30}, d_{50}, d_{60}, & U were obtained by conducting the gradation test. The experimental investigations included the computation of sand, gravel, and silt content, in addition to n and K values. Table 1 outlines the statistical summary of the experimental findings, highlighting the mean, maximum, minimum, and standard deviation. The soil samples analyzed have porosity values ranging from 0.286 to 0.426 and K values between 0.010 and 0.342 cm/s.

Table 1. Summary of key statistical parameters of soil sample characteristics.

Characteristics	Mean	Maximum	Minimum	Standard deviation
d_{10} (mm)	0.211	0.409	0.100	0.089
d_{30} (mm)	0.393	0.821	0.193	0.154
d_{50} (mm)	0.667	1.496	0.280	0.308
d_{60} (mm)	0.936	2.101	0.372	0.474
U^*	4.493	9.567	2.150	1.497
n*	0.362	0.426	0.286	0.029
Gravel (%)	7.050	31.240	2.200	4.430
Sand (%)	88.880	95.460	66.780	4.450
Silt (%)	4.070	7.340	1.130	1.430
K (cm/s)	0.069	0.342	0.010	0.061

** denotes the unitless characteristics.*

A correlation matrix was utilized to examine the relationship between the dependent parameter (K) and independent parameters i.e., d_{10}, d_{30}, d_{50}, d_{60}, n, and U. Table 2 presents that the d_{10} & d_{50} reveal a stronger correlation (0.94 and 0.80) in contrast to the weaker correlations (0.40 and 0.34) observed for d_{30} & d_{60} with the K value respectively. Meanwhile, the porosity and uniformity coefficient reveal a moderate correlation (Table 2) with the K value. Considering the correlation analysis, the d_{10}, d_{50}, n, and U are identified as the input variables for the development of the model.

Table 2. Correlation matrix for independent and dependent variables.

	d_{10}	**d_{30}**	**d_{50}**	**d_{60}**	**U**	**n**	**K**
d_{10}	1.00						
d_{30}	0.91	1.00					
d_{50}	0.84	0.93	1.00				
d_{60}	0.79	0.89	0.92	1.00			
U	-0.06	0.10	0.29	0.42	1.00		
n	0.02	-0.25	-0.30	-0.46	-0.93	1.00	
K	0.94*	0.40	0.80*	0.34	-0.58*	0.60*	1.00

**denotes the correlation that is statistically significant ($p<0.05$).*

For the model development and validation phase, the dataset was obtained by performing experiments on 165 porous media samples. Further, the data set was divided into 70% (115 soil samples) for model development and 30% (50 soil samples) for validation. A statistical overview of the input parameters i.e., d_{10}, d_{50}, U, & n, and output parameter (K) used in the development and validation phase is presented in Table 3.

Table 3. Summary of key statistical parameters of the data set used.

	Model development				Model validation			
Parameter	**Mean**	**Maximum**	**Minimum**	**Standard deviation**	**Mean**	**Maximum**	**Minimum**	**Standard deviation**
d_{10} (mm)	0.203	0.409	0.100	0.090	0.228	0.395	0.115	0.084
d_{50} (mm)	0.637	1.450	0.280	0.298	0.738	1.496	0.390	0.320
U*	4.466	9.567	2.150	1.544	4.554	8.323	2.498	1.387
n*	0.363	0.426	0.286	0.029	0.360	0.415	0.297	0.028
K (cm/s)	0.067	0.342	0.010	0.065	0.072	0.221	0.011	0.052

*** denotes the unitless variable.*

Hydraulic conductivity modelling using FFNN

The FFNN model was trained using the data points obtained from the 115 soil samples. A systematic trial-and-error evaluation of hidden-layer neuron configurations was undertaken to determine the FFNN model with the best performance. The most effective FFNN model, as identified by the analysis, features four inputs (d_{10}, d_{50}, U, & n), a hidden layer of five neurons, and an output variable, K. The FFNN model's accuracy in predicting K was analyzed through statistical measures and scatter plot visualization. Table 4 presents the statistical indicators corresponding to the best-performing FFNN model.

Table 4. Statistical indicators for FFNN, and KSOM models

Statistical Indicators	**FFNN model**		**KSOM model**	
	Development	**Validation**	**Development**	**Validation**
R^2	0.964	0.943	0.937	0.909
RMSE	0.012	0.016	0.018	0.024
SI	0.178	0.229	0.266	0.276
MBE	0.000	0.006	-0.002	-0.004
AI	0.980	0.977	0.975	0.902
MAE	0.006	0.007	0.010	0.012

Figure 7 depicts a scatter plot highlighting the comparison between FFNN-predicted and experimentally obtained K values during the development and validation stages. A strong correlation was observed between the FFNN-predicted and the measured K values, reflected by R^2 values of 0.96 and 0.94 in the development and validation phases, respectively. The validation results, as illustrated in Figure 7(b), indicate that the FFNN model performed well for K values below 0.10 cm/s and moderately for values above 0.10 cm/s. This suggests that the FFNN model had limited success in learning K values above 0.10 cm/s from the training data. The scatter in Figure 7 follows a consistent pattern along the 1-1 line, which was determined through linear regression between the measured K values and those predicted by the FFNN model. The regression line slope was not significantly different ($p > 0.05$) from the 1-1 line, suggesting that the FFNN model introduced minimal bias in K value predictions.

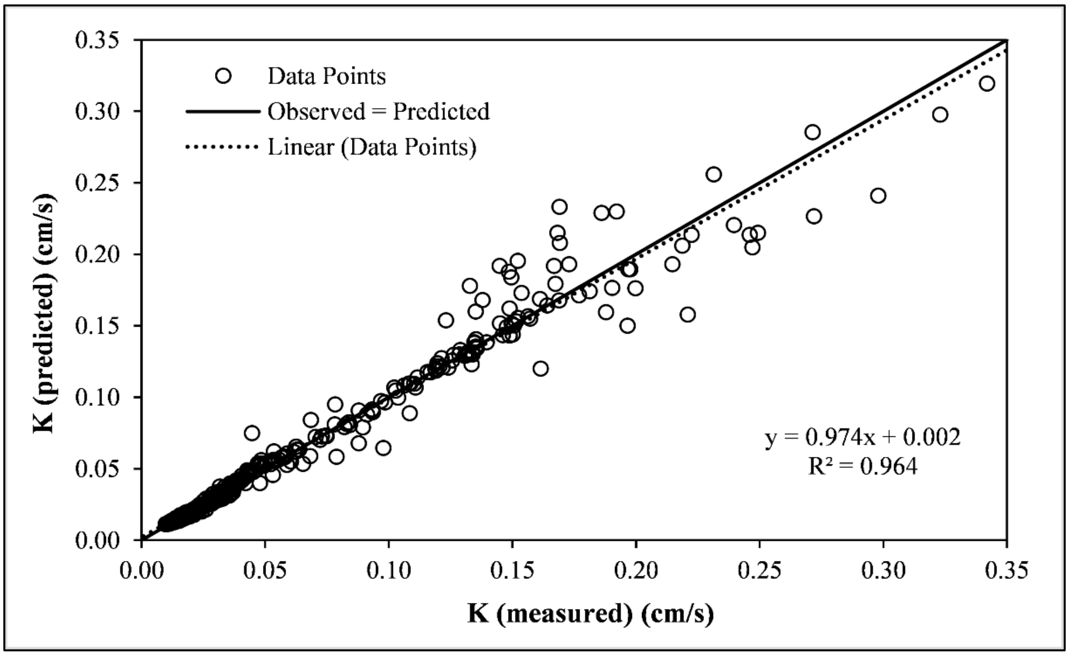

(a)

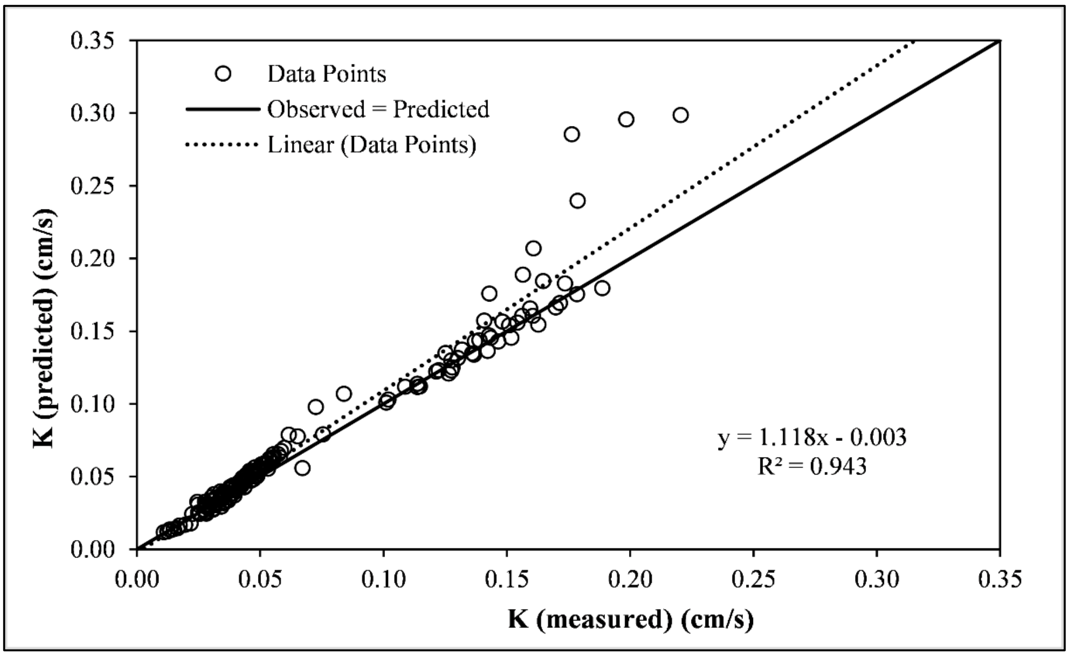

(b)

Figure 7. Scatter plot indicating the comparison between FFNN model predicted and measured K values during (a) development and (b) validation stages.

Hydraulic conductivity modelling using KSOM

Experimental findings from 115 and 50 soil samples were employed to develop and validate the KSOM model. The initial training of the KSOM model utilized default parameter values, setting the learning rate (λ) to 0.5, and defining the neighbourhood radius as $\alpha = \max(R_1, R_2)/4$, where R_1 and R_2 are the dimensions of the map. The SOM toolbox defines the final map dimensions, adjusting the total neuron count to the product of R_1 and R_2. The output map from the KSOM model has a size of 12×8, consisting of 96 units. One of the key advantages of KSOM is its potential to facilitate the visual examination of parameter correlations using component planes as presented in Figure 8.

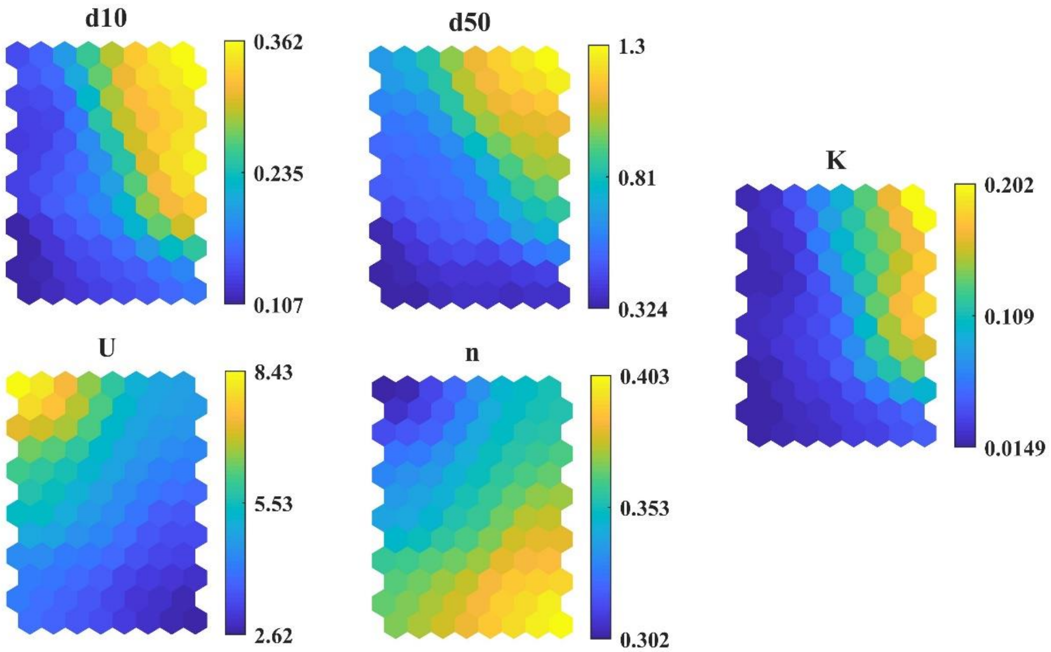

Figure 8. KSOM's component planes correspond to different parameters.

Each parameter is visualized on a component plane (Figure 8) made up of 96 hexagonal units, with values indicated through nearby colour coding. On the component plane, values are colour-coded as yellow for high, light blue for medium, and dark blue for low. Consequently, the component planes enhance visual clarity, allowing easier identification of regions with varying parameter levels. From Figure 8, it is evident that the colour gradient pattern of the d_{10} and d_{50} component planes run parallel to that of the K component plane, reflecting a correlation where low and high values of d_{10} and d_{50} correspond to low and high values of K, respectively. An inverse correlation between the U and n parameters is observed in their component planes, most prominently in the top-left and bottom-right regions, whereas, the central region of these parameters exhibits a consistent similarity in the colour gradient. Analysis of the component planes for U, n, and K indicates that the low K values on the top-left side are linked to low n and high U values. Conversely, higher K values on the top-right side correlate with medium n and U values. Also, examining the component planes in parts depicts distinct relationships between the parameters, yet a comprehensive assessment remains elusive.

The KSOM model efficacy to predict K was examined using statistical indicators (Table 4) and scatter plots (Figure 9) for both the development and validation stages.

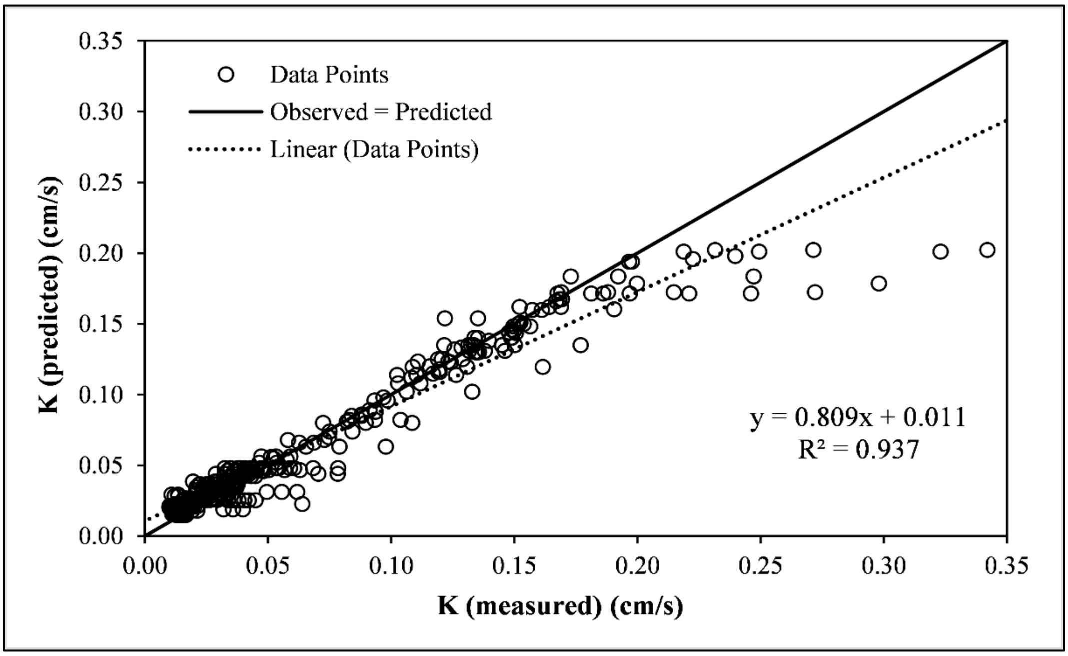

(a)

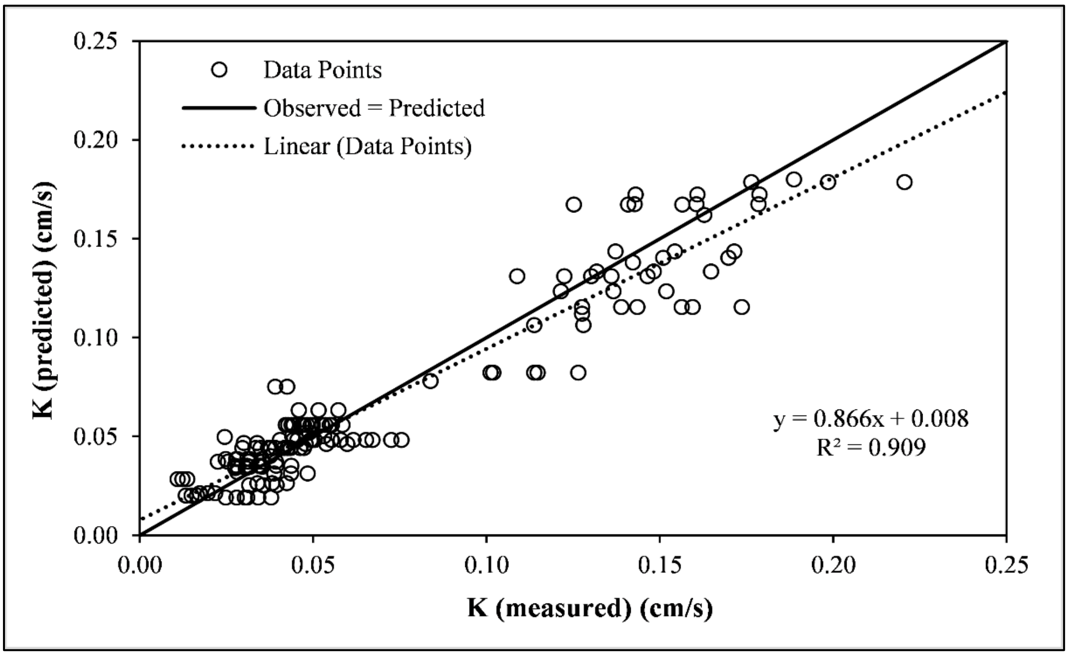

(b)

Figure 9. Scatter plot indicating the comparison between KSOM model predicted and measured K values during (a) development and (b) validation stages.

The KSOM model achieved an R^2 value of 0.91 during the validation stage, reflecting moderate prediction efficacy as shown in Figure 9(b). Also, the KSOM model demonstrated superior predictive accuracy (Figure 9b) for K values below 0.06 cm/s during validation, while its performance for values exceeding 0.06 cm/s was comparatively moderate. With a slope not statistically different from the 1:1 line ($p>0.05$) during both stages, the KSOM model exhibited low bias in predicting K. The low negative MBE values presented in Table 4 provide further confirmation of this finding.

Furthermore, a statistical comparison of the FFNN and KSOM models was carried out to ascertain which model provides a better estimate of the porous media's K. The statistical indicators presented in Table 4 indicate that the FFNN model outperforms the KSOM model in estimating the K values. The FFNN model achieved R^2 and AI values of 0.94 and 0.97 during validation, outperforming the KSOM model, which attained R^2 and AI values of 0.91 and 0.90, respectively. Additionally, the FFNN model's lower MBE, MAE, SI, and RMSE values (0.006, 0.007, 0.229, and 0.016, respectively) during validation underscore its efficacy in predicting the K of soil samples compared to the KSOM model.

Conclusions

The study evaluates the predictive potential of FFNN and KSOM models for determining the hydraulic conductivity of porous media. Correlation analysis suggests that K is predominantly influenced by porosity, uniformity coefficient, and grain-size namely d_{10} & d_{50}. The performance of both models i.e., FFNN and KOSM was examined using scatter plots and statistical indicators. The FFNN model outperforms the KSOM model in estimating K of soil samples during the development and validation stages, highlighting its effectiveness as the best-performing model. The KSOM model demonstrates satisfactory results for estimating K during development; however, its validation performance is comparatively moderate. The FFNN model achieved higher R^2 and AI values of 0.94 and 0.97, respectively, compared to the KSOM model during validation, emphasizing the prediction efficacy of the FFNN model in computing the K value. The study highlights the potential of these techniques and encourages their application in future research on K estimation for diverse soil samples.

References

Adeloye, A. J., Rustum, R. & Kariyama, I. D. 2011 Kohonen self-organizing map estimator for the reference crop evapotranspiration. *Water Resources Research* **47**(8), 1-19.

Akbulut, S. 2005. Artificial neural networks for predicting the hydraulic conductivity of coarse-grained soils. *Eurasian Soil Science* **38**(4), 392-398.

Arshad, R. R., Sayyad, G., Mosaddeghi, M. & Gharabaghi, B. 2013 Predicting saturated hydraulic conductivity by artificial intelligence and regression models. *International Scholarly Research Notices* **2013**, 1-8.

ASTM 2006 Standard D2434 - Permeability of granular soils (Constant head). West Conshohocken, PA, USA.

ASTM 2007 Standard D422 – Particle-Size Analysis of Soils. ASTM International, West Conshohocken, PA, USA.

Chandel, A. & Shankar, V. 2022 Evaluation of empirical relationships to estimate the hydraulic conductivity of borehole soil samples. *ISH Journal of Hydraulic Engineering* **28**(4), 368-377.

Chandel, A., Fayaz, F. & Shankar, V. 2022a Assessment of column to particle diameter ratio on the hydraulic conductivity of porous media: Wall effect in Darcy Regime. *ISH Journal of Hydraulic Engineering*, 1-9.

Chandel, A., Sharma, S. & Shankar, V. 2022b Prediction of hydraulic conductivity of porous media using a statistical grain-size model. *Water Supply* **22**(4), 4176-4192.

Dawson, C. W. & Wilby, R. L. 2001 Hydrological modelling using artificial neural networks. *Progress in physical Geography* **25**(1), 80-108.

Elbisy, M. S. 2015 Support vector machine and regression analysis to predict the field hydraulic conductivity of sandy soil. *KSCE Journal of Civil Engineering* **19**, 2307-2316.

Garcia, H. L. & Gonzalez, I. M. 2004 Self-organizing map and clustering for wastewater treatment monitoring. *Engineering applications of artificial intelligence* **17**(3), 215-225.

Kohonen, T., Oja, E., Simula, O., Visa, A. & Kangas, J. 1996 Engineering applications of the self-organizing map. *Proceedings of the IEEE* **84**(10), 1358-1384.

Kumar, N., Adeloye, A. J., Shankar, V. & Rustum, R. 2020 Neural computing modelling of the crop water stress index. *Agricultural Water Management* **239**, p.106259.

Kumar, N., Shankar, V., Rustum, R. & Adeloye, A. J. 2021 Evaluating the performance of self-organizing maps to estimate well-watered canopy temperature for calculating crop water stress index in Indian mustard (Brassica Juncea). *Journal of Irrigation and Drainage* Engineering **147**(2), p.04020040.

Lee, B. J., Lee, J. H., Yoon, H. & Lee, E. 2015 Hydraulic experiments for determination of in-situ hydraulic conductivity of submerged sediments. *Scientific reports* **5**(1), 1-5.

Lu, C., Chen, X., Cheng, C., Ou, G. & Shu, L. 2012 Horizontal hydraulic conductivity of shallow streambed sediments and comparison with the grain-size analysis results. *Hydrological Processes* **26**(3), 454-466.

Naeej, M., Naeej, M. R., Salehi, J. & Rahimi, R. 2017 Hydraulic conductivity prediction based on grain-size distribution using M5 model tree. *Geomechanics and Geoengineering* **12**(2), 107-114.

Naganna, S. R. & Deka, P. C. 2019 Artificial intelligence approaches for spatial modeling of streambed hydraulic conductivity. *Acta Geophysica* **67**, 891-903.

Odong, J. 2007 Evaluation of empirical formulae for determination of hydraulic conductivity based on grain-size analysis. *Journal of American Science* **3**(3), 54-60.

Penn, B. S. 2005 Using self-organizing maps to visualize high-dimensional data. *Computers & Geosciences* **31**(5), 531-544.

Pucko, T. & Verbovsek, T. 2015 Comparison of hydraulic conductivities by grain-size analysis, pumping, and slug tests in Quaternary gravels, NE Slovenia. *Open Geosciences* **1**, 308-317.

Qiu, Z. F. & Wang, J. J. 2015 Experimental study on the anisotropic hydraulic conductivity of a sandstone–mudstone particle mixture. *Journal of Hydrologic Engineering* **20**(11), 1-9.

Riha, J., Petrula, L., Hala, M. & Alhasan, Z. 2018 Assessment of empirical formulae for determining the hydraulic conductivity of glass beads. *Journal of Hydrology and Hydromechanics* **66**(3), 337-347.

Rustum, R. & Adeloye, A. J. 2007 Replacing outliers and missing values from activated sludge data using Kohonen self-organizing map. *Journal of Environmental Engineering* **133**(9), 909-916.

Sen, D., Aghazadeh, A., Mousavi, A., Nagarajaiah, S., Baraniuk, R. & Dabak, A. 2019 Data-driven semi-supervised and supervised learning algorithms for health monitoring of pipes. *Mechanical Systems and Signal Processing* **131**, 524-537.

Thakur, D., Chandel, A. & Shankar, V. 2022 Estimation of hydraulic conductivity of porous media using data-driven techniques. *Water Practice & Technology* **17**(12), 2625-2638.

Wang, J. P., François, B. & Lambert, P. 2017 Equations for hydraulic conductivity estimation from particle size distribution: A dimensional analysis. *Water Resources Research* **53**(9), 8127-8134.

Williams, C. G. & Ojuri, O. O. 2021 Predictive modelling of soils' hydraulic conductivity using artificial neural network and multiple linear regression. *SN Applied Sciences* **3**, 1-13.

Yilmaz, I., Marschalko, M., Bednarik, M., Kaynar, O. & Fojtova, L. 2012 Neural computing models for prediction of permeability coefficient of coarse-grained soils. *Neural Computing and Applications* **21**, 957-968.